ELSEVIER

Infrared Physics & Technology 42 (2001) 157–162

INFRARED PHYSICS & TECHNOLOGY

www.elsevier.com/locate/infrared

35 μm cutoff bound-to-quasibound and bound-to-continuum InGaAs QWIPs

A.G.U. Perera [a,*], S.G. Matsik [a], H.C. Liu [b], M. Gao [b], M. Buchanan [b], W.J. Schaff [c], W. Yeo [c]

[a] *Department of Physics and Astronomy, Georgia State University, Atlanta, GA 30303, USA*
[b] *Institute for Microstructural Sciences, National Research Council, Ottawa, Ont., Canada K1A 0R6*
[c] *School of Electrical Engineering, Cornell University, Ithaca, NY 14853, USA*

Abstract

GaAs/InGaAs far-infrared quantum well photodetectors based on a bound-to-continuum (bc) and bound-to-quasibound (bq) intersubband transition with a cutoff wavelength (zero response) up to 35 μm are reported. A peak responsivity of 0.45 and 0.30 A/W and detectivity of 6×10^9 and 1.0×10^{10} cm $\sqrt{\text{Hz}}$/W at a wavelength of 31 μm and a temperature of 4.2 K respectively for a bc and a bq detector have been achieved.

PACS: 78.66.Fd; 85.30.De; 85.60.Gz

1. Introduction

Quantum well infrared photodetectors (QWIPs) have attracted attention [1] for applications where their high detectivity, extremely good uniformity, radiation hardness and low power consumption are useful properties. Infrared cameras have already been developed based on QWIP arrays operating at wavelengths around 10 μm [2]. Cutoff wavelengths for QWIPs have been extended out to 28 μm for AlGaAs [3]. A 35 μm InGaAs bound-to-continuum (bc) detector was reported very recently [4]. Wide range wavelengths for QWIPs would be important for space applications in infrared astronomy and satellite mapping, where the arrays would provide a useful alternative to the currently available Ge detectors with detectivities in the range 10^9–10^{14} cm $\sqrt{\text{Hz}}$/W [5]. In this paper results are presented on InGaAs QWIPs based on bound-to-quasibound (bq) and bc transitions with response wavelengths in the range 30–35 μm.

2. Device structure

Two samples were used to investigate long wavelength response for InGaAs QWIPs. The sample designs were similar except for the well width, with one sample, R040 giving a bc transition while the other sample, R041 gives a bq transition. For both samples the wells were $In_{0.087}Ga_{0.913}As$ while the barriers were GaAs. Both structures had 20 periods and an undoped GaAs buffer was grown between the contacts and

* Corresponding author. Tel.: +1-404-651-2709; fax: +1-404-651-1427.
E-mail address: uperera@gsu.edu (A.G.U. Perera).

1350-4495/01/$ - see front matter
PII: S1350-4495(01)00071-8

Table 1
The well (w), barrier (b), and buffer (t) thicknesses of the two samples with the ground (E_0) and first excited (E_1) state energies for the samples

Sample	w (Å)	b (Å)	t (Å)	E_0 (meV)	E_1 (meV)
R040	83 ± 4	338 ± 15	423 ± 20	24	59.5
R041	98 ± 4	334 ± 15	418 ± 20	20.5	56.5

the end wells to form the contact barriers. The thicknesses of the various layers and the ground and first excited state energies are given in Table 1. The wells were δ doped with Si to 4.0×10^{10} cm^{-2} and the contacts were doped to 1×10^{18} cm^{-3}. The band diagram is shown in Fig. 1 for the structure at zero bias. The triangular shape of the contact barriers is due to band bending between the doped GaAs and the InGaAs wells. The outer barrier between wells also has a nonzero field due to the increased Fermi energy of the outer well resulting from the band bending. The QWIP peak wavelengths expected from the energy levels determined from the Kronig–Penny model using the nominal device parameters would be 34 μm for sample R040 and 35 μm for sample R041. The corresponding experimental peaks were observed at 31 μm for both samples with a (zero response) cutoff at 35 μm under back illuminated conditions. For

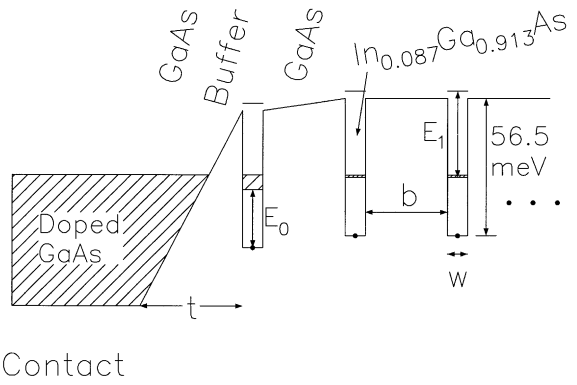

Fig. 1. Structure designed for the GaAs/InGaAs QWIPs. The barriers of thickness b were GaAs and the wells of thickness w had an In fraction of 0.087 δ doped to 4×10^{10} cm^{-2} with Si. Buffer regions of thickness t adjacent to the first and last wells served as contact barriers and the contacts were Si doped to 1×10^{18} cm^{-3}. The values of w, b, and t and the ground and excited state energies E_0 and E_1 are given in Table 1. The energy levels shown correspond to sample R040.

wavelengths in the range 35–40 μm, there is strong reststrahlen absorption in the substrate, masking the true response peak in the structures. Two phonon absorption in the substrate can be reduced by the use of front illumination with a grating structure to couple the radiation to the QWIP [2]. However the reststrahlen effects will still be observed under front illumination.

3. Dark current

The GaAs/InGaAs far-infrared (FIR) QWIPs were fabricated by etching 240×240 μm^2 mesas using conventional wet chemical etching techniques. Ni/Ge/Au ohmic contacts were evaporated onto the top and bottom layers. The dark current–voltage curves measured at different temperatures for sample R040 and at 4.2 K for sample R041 as shown in Fig. 2 are highly symmetric indicating negligible dopant migration in the well [6]. Minimal dopant migration was expected due to the low growth temperature (~500°C) for InGaAs.

The dark current showed two different regimes. A tunneling and field assisted tunneling regime below 25 K where the dark current slowly increased with temperature, and a thermionic emission dominated regime above 25 K where the dark current increased rapidly. The activation energies obtained from Arrhenius plots as shown in the insets in Fig. 2 (and the values expected from the parameters) were $\sim 18 \pm 4$ meV (31.5 meV expected) for sample R040 and $\sim 14 \pm 4$ meV (35.5 meV expected) for sample R041. The deviation between the experimental activation energy and the expected value obtained from the difference between the top of the Fermi sea for the ground state and the top of the barrier based on the nominal parameters is believed to be due to the effects of impurities in the barriers [4].

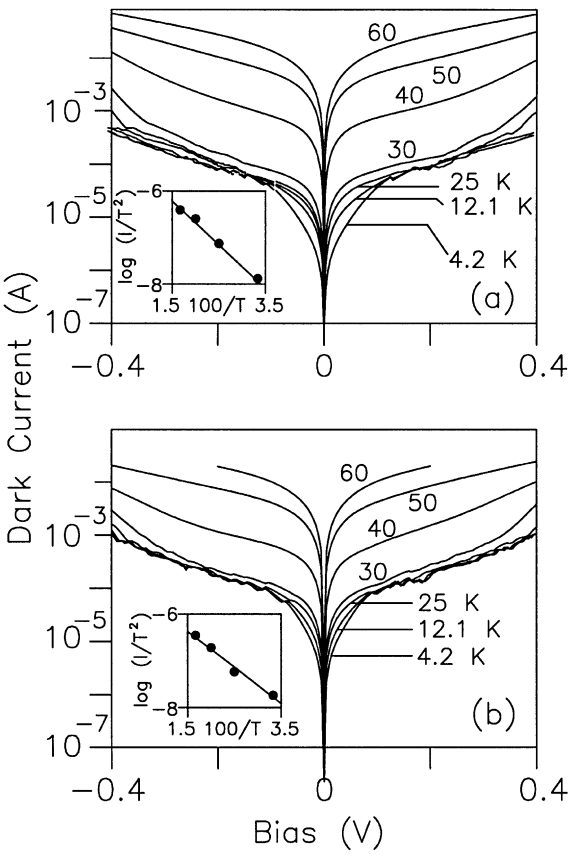

Fig. 2. (a) Dark current vs bias voltage curves at different temperatures for sample R040. Positive bias means top positive. The inset shows an Arrhenius plot from which the effective value of $\Delta = 18 \pm 4$ meV for injection was obtained. (b) Dark current at various temperatures for sample R041. The inset shows the Arrhenius plot used to obtain the effective activation energy of 14 ± 4 meV.

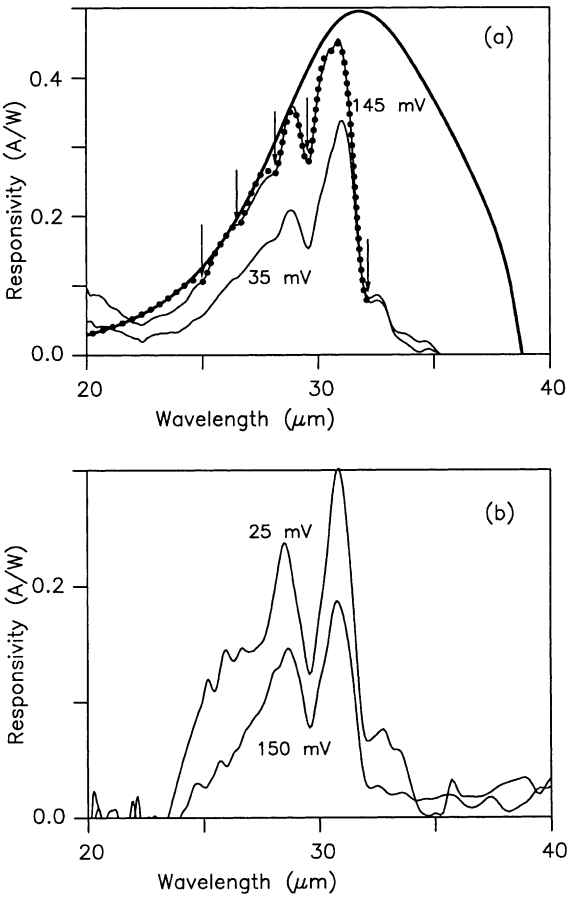

Fig. 3. (a) Measured and calculated spectral response of sample R040 measured at 4.2 K under different bias values. The valleys indicated by the vertical arrows at 26.6, 28.3, 29.6 and 32.3 μm are due to two phonon absorption of GaAs substrate [8]. The thick line shows a calculated response determined using an intersubband transition from a 24 meV ground state to a 60 meV first excited state with a barrier of 56.5 meV. The dotted curve is the theoretical response corrected for the two phonon absorptions indicated. Note the almost exact fit to the 145 mV bias experimental response. A similar curve could be obtained for 35 mV bias. (b) Measured spectral response of sample R041 at 4.2 K under different bias values. The peak response may be masked in this case due to the predicted peak response occurring at the substrate absorption maximum near 35 μm.

4. Responsivity and detectivity

The responsivity spectra of the detectors were measured using a Perkin–Elmer, system 2000, Fourier transform infrared spectrometer (FTIR). The detectors were back illuminated through a 45° polished facet and a Si composite bolometer was used as the reference detector to obtain the background spectrum and the responsivity. Sample R040 showed response up to 35 μm with peak responsivity at 31 μm as shown in Fig. 3(a) for 35 and 145 mV bias values at 4.2 K. The highest measured responsivity was 0.45 A/W at a bias of 0.145 V. The thick line in Fig. 3(a) shows the calculated response for a bc intersubband transition using the model of Choi [7]. The energy levels and the barrier height used were obtained from the

nominal device parameters. The multiphonon absorption in the substrate [8] is indicated by the vertical arrows at 26.6, 28.3, 29.6 and 32.3 μm. The calculated response was then corrected for the multiphonon absorptions by using gaussian absorption features centered on the multiphonon lines producing a model response that almost exactly matches the experimental response at 145 mV [4] (see the dotted line in Fig. 3).

The response for the bq detector is shown in Fig. 3(b). In this case the responsivity is expected to show a Lorentzian lineshape with the same absorption lines as were present for the other sample. The peak responsivity of 0.3 A/W was seen at 31 μm for a bias of 25–50 mV. The peak of the response based on the nominal device parameters is expected to be 35 μm which is at the peak of the reststrahlen absorption. Because of the strong absorption at the peak wavelength a fit to the lineshape is not possible so the ideal peak response could not be obtained as was done for sample R041. The fact that the responsivity goes to zero at shorter wavelengths indicates that the excited state is at or slightly below the top of the barrier.

The intersubband transition was confirmed by measuring the polarization dependence of the photoconductivity signal for sample R040 [4]. The voltage dependence of the response for both detectors is shown in Fig. 4 which rises to a maximum and then remains relatively constant for sample R040 as is typical of QWIPs. For sample R041 the response was low at 10 mV rising to a maximum at 25–50 mV and then decreasing. Based on the nominal device parameters it is believed that the bottom of the excited state is below the barrier while the top of the excited state is above the barrier. The decrease at larger bias may be due to drift velocity changes in the barriers.

Noise was measured using a low-noise preamplifier (SR560) and a fast Fourier transform (FFT) spectrum analyzer (SR780) with the detector at 4.2 K. The noise spectra showed no frequency dependence and had a value of $S_i = 3.4 \times 10^{-24}$ A^2/Hz at a bias of 145 mV for sample R040 and 4.0×10^{-25} A^2/Hz for sample R041 at all biases. The noise in sample R040 showed a minute variation from 3.2 to 3.5×10^{-24} A^2/Hz as the bias

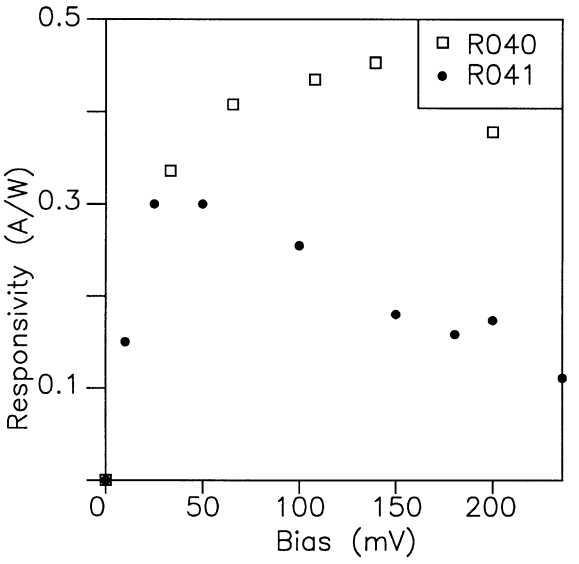

Fig. 4. The responsivity vs bias at 31 μm for both samples sample R040 showed a relatively constant response with bias as is expected for a QWIP while R041 showed a decreasing response possibly due to drift velocity variations in the barriers.

was increased from 0 to 200 mV. This lack of noise variation with bias is an indication that the primary noise source is not generation–recombination noise. Using the measured noise and peak responsivities, the noise equivalent power (NEP) was found from $\mathrm{NEP} = \sqrt{S_i}/R$ to be 4.0×10^{-12} $\mathrm{W}/\sqrt{\mathrm{Hz}}$ giving $D^* = 6.0 \times 10^9$ $\mathrm{cm}\sqrt{\mathrm{Hz}}/\mathrm{W}$ as a conservative estimate for R040. The calculated spectrum without absorption gives $D^* = 6.6 \times 10^9$ $\mathrm{cm}\sqrt{\mathrm{Hz}}/\mathrm{W}$. For sample R041 the NEP was 2.4×10^{-12} $\mathrm{W}/\sqrt{\mathrm{Hz}}$ giving $D^* = 1.0 \times 10^{10}$ $\mathrm{cm}\sqrt{\mathrm{Hz}}/\mathrm{W}$. The detectivity in this sample may be higher as the predicted peak response would be masked by the strong absorption in the substrate. Relating the expected dark current shot noise to the measured noise by $S_i = 4qI_d g$, where q is the electron charge, I_d is the dark current and g the optical gain is obtained as $g = 0.11$ for sample R041 and $g = 0.012$ for R040. The gain values are lower than is expected for QWIPs indicating the presence of a leakage current [9] and are consistent with the primary noise source not being g–r noise. Once tunneling and defect related current is reduced the NEP and D^* should be improved.

5. Capacitance

Shown in Fig. 5 is a plot of capacitance vs bias at 1 MHz and 4.2 K for biases below 0.2 V for samples R040 and R041. The capacitance at zero bias is near the geometrical capacitance and slowly decreases as the bias is increased. For sample R040 the capacitance remains positive while for sample R041 the capacitance becomes negative for biases above 150 mV. The presence of negative capacitance has been associated with interface states [10] and with intrinsic transport processes [11] in other detectors. Also observed on both samples are several large spikes occurring at bias values where negative differential conductance is observed in the I–V curve. The capacitance spikes and negative differential conductance were related to tunneling effects [12] which become significant even for thick barriers due to the low barrier height [4]. The resonances are more sensitive to small variations in the device which provides a possible explanation for the asymmetry in the peak positions. The amplitude of the spikes increases with decreasing frequency while the conductance remained constant.

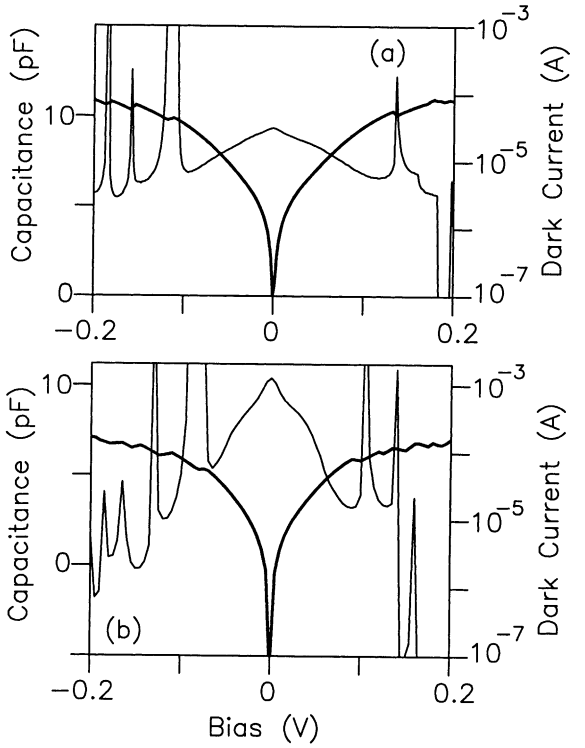

Fig. 5. Capacitance vs voltage (thin curve) for a frequency of 1 MHz and current vs voltage (thick curve) for (a) sample R040 and (b) sample R041 at 4.2 K. The spikes in capacitance correspond to the biases where negative differential conductivity is observed. Similar C–V curves were obtained for frequencies above 20 kHz.

6. Conclusion

In summary, FIR quantum well photodetectors which are based on bc and bq intersubband transitions of GaAs/$In_xGa_{1-x}As$ are reported. A peak responsivity of 0.45 A/W and detectivity of 6.0×10^9 cm$\sqrt{\text{Hz}}$/W and NEP of 4.0×10^{-12} W/$\sqrt{\text{Hz}}$ from noise measurements at 4.2 K have been achieved for the bc case and peak responsivity of 0.3 A/W and detectivity of 1.0×10^{10} cm$\sqrt{\text{Hz}}$/W and NEP of 2.4×10^{-12} W/$\sqrt{\text{Hz}}$ for the bq case. Detector response was observed at temperatures up to 18 K for the bc detector. The detectivity of the bq detector was lower than that of the bc detector. This may be due to the predicted peak occurring at the maximum of absorption in the substrate. In spite of this difference the detectivity of the bq detector was still higher than the bc detector. It is expected that elimination of impurities in the material will lead to improved detector performance.

Acknowledgements

This work was supported in part by the NSF under grant no. ECS-98-09746. The work at NRC was supported in part by DND. The authors acknowledge S.J. Rolfe for SIMS measurements.

References

[1] B.F. Levine, J. Appl. Phys. 74 (1993) R1.
[2] S.D. Gunapala, S.V. Bandara, Quantum well IR photodetector focal plane arrays, in: H.C. Liu, F. Capasso, Semiconductors and Semimetals, vol. 62, Academic Press, New York, 2000, pp. 197–291.

[3] A.G.U. Perera, W.Z. Shen, S.G. Matsik, H.C. Liu, M. Buchanan, W.J. Schaff, Appl. Phys. Lett. 72 (1998) 1596.
[4] A.G.U. Perera, S.G. Matsik, H.C. Liu, M. Gao, M. Buchanan, W.J. Schaff, W. Yeo, Appl. Phys. Lett. 77 (2000) 31.
[5] P.W. Pellegrini, J.R. Jimenez, Thin film epitaxial layers on silicon for the detection of infrared signals, The Physics of Thin Films, vol. 23, Academic Press, New York, 1998, p. 115.
[6] H.C. Liu, Z.R. Wasilewski, M. Buchanan, H. Chu, Appl. Phys. Lett. 63 (1993) 761.
[7] K.K. Choi, The Physics of Quantum Well Infrared Photodetectors, World Scientific, Singapore, 1997.
[8] E.S. Koteles, W.R. Datars, Can. J. Phys. 54 (1976) 1676.
[9] H.C. Liu, Appl. Phys. Lett. 60 (1992) 1507.
[10] A.G.U. Perera, W.Z. Shen, M. Ershov, H.C. Liu, M. Buchanan, W.J. Schaff, Appl. Phys. Lett. 74 (1999) 3167.
[11] M. Ershov, H.C. Liu, L. Li, M. Buchanan, Z.R. Wasilewski, A.K. Jonscher, IEEE Trans. Electron. Dev. 45 (1998) 2196.
[12] J. Li, H.C. Liu, M. Buchanan, Z.R. Wasilewski, J.G. Simmons, J. Appl. Phys. 75 (1994) 1748.